Scalp attached tangential magnetoencephalography using tunnel magneto-resistive sensors

Akitake Kanno
Tohoku University Graduate School of Medicine
Nobukazu Nakasato (nkst@med.tohoku.ac.jp)
Tohoku University Graduate School of Medicine
Mikihiko Oogane
Tohoku University
Kosuke Fujiwara
Spin Sensing Factory Corp
Takafumi Nakano
Tohoku University
Tadashi Arimoto
KONICA MINOLTA, INC
Hitoshi Matsuzaki
Tohoku University
Yasuo Ando
Tohoku University

Research Article

Keywords: scalp, sensors, invasive, brain, functional

Posted Date: November 12th, 2021

DOI: https://doi.org/10.21203/rs.3.rs-1045724/v1

Version of Record: A version of this preprint was published at Scientific Reports on April 12th, 2022. See the published version at https://doi.org/10.1038/s41598-022-10155-6.

Abstract

Non-invasive human brain functional imaging with millisecond resolution can be achieved only with magnetoencephalography (MEG) and electroencephalography (EEG). MEG has better spatial resolution than EEG because signal distortion due to inhomogeneous head conductivity is negligible in MEG but serious in EEG. However, this advantage has been practically limited by the necessary setback distances between the sensors and scalp, because the Dewar vessel containing liquid helium for superconducting sensors requires a thick vacuum wall. Latest developments of high critical temperature (high-T_c) superconducting or optically pumped magnetometers have not allowed scalp-attached MEG due to cold or hot temperatures at the sensing point, respectively. Here we applied tunnel magneto-resistive (TMR) sensors that operate at room temperature. Improvement of TMR sensitivity with magnetic flux concentrators enabled scalp-attached and scalp-tangential MEG to target the largest signal component produced by the neural current below. In a healthy subject, our single-channel TMR-MEG system clearly demonstrated the N20m, the initial cortical component of the somatosensory evoked response after median nerve stimulation. Multisite measurement confirmed a spatially and temporally steep peak of N20m, immediately above the source at a latency around 20 ms, indicating a new approach to non-invasive functional brain imaging with millimeter and millisecond resolutions.

Introduction

EEG and MEG are the only methods of non-invasive imaging of human brain function that can achieve millisecond time resolution by electrical or magnetic neural current measurement[1]. MEG has theoretically higher spatial resolution than EEG because MEG suffers negligible signal distortion due to inhomogeneous head conductivity, whereas EEG shows serious distortion[1,2]. However, the spatial resolution of MEG has been practically limited by the necessary setback distance between the sensors and scalp. The development of MEG sensors attached to the scalp has long been a target of research because magnetic field strength attenuates according to the square root law of sensor-source distance[3].

Conventional MEG sensors, generally called superconducting quantum interference devices (SQUIDs), require ultra-low operating temperatures (-269˚C) only achieved by liquid helium, so a Dewar vessel with thick vacuum walls is required to contain the liquid helium and the sensors[1,2]. Another problem is the construction of the helmet-shaped Dewar vessel to cover the entire head. The fixed shape greatly increases the setback distance, in order to accommodate the individual variability in head size and shape[1,2]. Latest developments in high-T_c superconducting[4,5] or optically pumped[6,7] magnetometers have not allowed scalp-attached MEG due to cold or hot temperatures at the sensing point, respectively.

Here we introduce the use of TMR sensors based on magnetic tunnel junctions (MTJs) that operate at room temperature[8,9]. We have already reported successful measurement of chest-attached magnetocardiography (MCG) without signal averaging techniques and scalp-attached MEG of the alpha wave, awake brain background rhythm, by signal averaging techniques[10]. Our combination of magnetic

flux concentrators has finally reached to the sensitivity of the TMR sensor at the level of 940 fT/√Hz at 1 Hz and 50 fT/√Hz at 1 kHz, which are adequate to measure somatosensory evoked magnetic fields (SEFs), which are one of the weakest signals but used in most common applications of MEG[11-14]. Our present success with scalp-attached tangential MEG measurement will allow non-invasive imaging of human brain functions at millimeter and millisecond resolutions.

Tmr Sensors.

Figure 1 shows our TMR sensor system for scalp-attached tangential MEG. The core of the TMR sensor consists of MTJs developed based on recent spintronics science[8,9]. At room temperature, the magnetic field can be measured as resistance change through MTJs. Recently, marked improvement in the sensitivity has enabled us to perform MCG even without signal averaging techniques, as well as detect the MEG signal of the alpha rhythm, background brain activity during wakefulness, with averaging techniques in a healthy subject[10]. We have now dramatically improved the signal-to-noise ratio of the TMR sensor by optimizing the film structure of the MTJs, integrating the MTJ devices, combining a facing pair of T-shaped magnetic flux concentrators (MFCs), and developing a low-noise amplifier circuit. The sensitivity of our new TMR sensor has achieved the level of 940 fT/√Hz at 1 Hz, 200 fT/√Hz at 10 Hz, and 50 fT/√Hz at 1 kHz, which is about 100 times the sensitivity of previous magneto-resistive sensors[15]. Our TMR sensor is especially suitable for biomagnetic signals, such as those of MEG, with very weak amplitude and low frequencies, in contrast to the other highly sensitive magnetic sensor devices, such as magneto-impedance sensors[16], fluxgate sensors[17], or diamond quantum sensors[18].

Advantages of scalp “tangential” MEG.

Figure 2 compares the radial and tangential measurements of MEG, simulating the conventional SQUID-MEG system and our TMR-MEG system, respectively, for different sensor positions on the scalp. Isofield maps of the N20m, the initial cortical component of SEF after median nerve stimulation, were calculated based on actually measured data using a helmet-shaped MEG system with 200 channel SQUID sensors (Fig. 3c–e). The shorter setback distance between the MEG sensors and the scalp obtained larger signal amplitude and more localized signal distribution in both radial and tangential maps.

In the radial maps simulating conventional SQUID-MEG measurements (Fig. 2b), a single tangential neural current produces the null field at the scalp immediately above the source, but a pair of outflux and influx peaks, called the single dipole pattern, spatially separated according to the distance function between the sensors and the source[2]. Mathematical models are necessary to estimate the location and orientation of the neural current underneath the scalp[2]. If there are two or more neural sources, separation of these sources becomes difficult in radial MEG because the multiple dipole patterns spatially overlap. In conventional radial MEG systems, the pickup coil surfaces have setback distances of 20 mm or more. Consequently, separation of multiple sources has been challenging in many MEG applications, especially for clinical use, unless only two or a limited number of sources are separated far enough for visual

separation[19,20] or the use of highly sophisticated mathematical models with certain limitations for nearby sources[21].

In the tangential maps simulating our new TMR-MEG (Fig. 2c), a single tangential neural current produces the highest signal intensity at the scalp immediately above the source as the sensing axis is set perpendicularly to the source current. Mathematical models may not be necessary to identify the scalp position immediately above the source if the multisite measurement (Fig. 3b) is available or a high-density multichannel system could be used in the future.

Demonstration of scalp surface and scalp tangential TMR-MEG.

We measured the SEFs for left median nerve stimuli using a newly developed TMR sensor in a subject (Fig. 3a–c). Based on the N20m source position and orientation previously estimated by SQUID-MEG (Fig. 3d, e), we placed a TMR sensor on the right parietal scalp directly to measure the tangential component of MEG (Fig. 3a). The sensing axis of the sensor was set to measure perpendicular, parallel, and opposite perpendicular components to the N20m current orientation. We confirmed clear and reproducible N20m peaks and the following P30m components of the SEF tangentially to the scalp. These waveforms were almost identical to the radial components of N20m and P30m measurements obtained by SQUID-MEG (Fig. 3c). Then we placed the TMR sensor at 10 different grid sites at 5-mm distances to visualize the isofield map of the tangential N20m over the scalp (Fig. 3b) and found a spatially steep peak of N20m confirming our previous simulation (Fig. 2c).

Discussion

The present study succeeded in scalp-attached and scalp-tangential measurement of SEFs using a newly developed TMR sensor that operates at room temperature. Multisite measurement using the single channel TMR sensor identified a spatially steep N20m peak immediately above the source, showing higher spatial resolution than conventional SQUID-MEG systems. Our findings indicate the potential of TMR-MEG for non-invasive functional brain imaging with millimeter and millisecond resolutions.

TMR has several known advantages which may allow revolutionary development of MEG for functional human brain imaging and clinical application[22]. First, the wide dynamic range above 100 μT of our TMR sensors may enable MEG measurement outside the magnetically shielded room, as we already demonstrated in MCG measurement. Second, the fabrication and running costs of TMR sensors are far lower than any other biomagnetic sensors[23]. Third, the MTJs, the core of the TMR sensors, are much smaller than any other biomagnetic sensors, i.e., as small as 50 μm. Further improvement of sensitivity of the TMR magnetometer may enable use of even smaller MFCs or even without MFCs. Spatial resolution of MEG depends on sensor spacing: smaller distance between the sensors provides better discrimination between neural sources[5].

Tangential measurement is another advantage of TMR-MEG, which detects the largest signal component of MEG produced by the current below, and because the fixed sensing axis of the TMR sensor can detect neural current orientation below the sensor. In the future, high density arrangement of small TMR sensors with orthogonal sensing axes will be able to clearly separate and localize multiple neural activities. For already known multiple neural activities, a limited number of TMR sensors can be placed on the scalp immediately above the sources with tangential sensing axis to the scalp and perpendicular sensing axis to each current orientation.

In conclusion, our present success with scalp-attached and scalp-tangential MEG measurement will allow the development of non-invasive imaging of functional human function with millimeter and millisecond resolutions.

Methods

Subject.

A right-handed male subject, aged 27 years at the time of participation, was recruited from local residents through advertisements in a local town paper. The subject was not using any medications known to interfere with cognitive function, including benzodiazepines, antidepressants, or other central nervous system agents. He had no history of head trauma, mental disease, or diseases known to affect the central nervous system. This study was approved by the Ethics Committee of the Tohoku University Graduate School of Medicine for the SQUID-MEG part (#2021-21650) and Graduate School of Engineering for the TMR-MEG part (#2018-17A-16). Written informed consent was obtained from a subject. The study was conducted according to the principles expressed in the Declaration of Helsinki.

SEFs using SQUID-MEG.

Electrical stimulation was administered to the left median nerve of the subject. The electrical stimuli consisted of constant current biphasic pulses with duration of 0.3 ms delivered at 2.9 Hz. Stimulus intensity was set at 1.5 times the motor threshold to evoke a twitch of the thumb[24].

SEFs were recorded in a magnetically shielded room using a 200-channel whole-head type axial gradiometer system (MEGvision PQA160C-RO; Ricoh, Tokyo, Japan). The sensors are configured as first-order axial gradiometers with a baseline of 50 mm; each gradiometer coil is 15.5 mm in diameter. The sensors are arranged in a uniform array on a helmet-shaped surface at the bottom of a Dewar vessel, and the mean distance between the centers of two adjacent coils is 25 mm. Sensor field sensitivity (noise of the system) was 3 fT/Hz within the frequency range for SEFs[25,26]. The subjects lay supine, with the head location determined by the positions of five fiduciary markers consisting of induction coils placed at known locations on the scalp. The head shape and coil positions were established using a three-dimensional digitizer (Fast SCAN Cobra; Polhemus, Inc., Colchester, VT) based on three-dimensional MR images obtained for all subjects using a 3T MR system (Achieva; Philips Healthcare, Best, the Netherlands). The MEG signal was band-pass filtered between 0.03 Hz and 2,000 Hz and sampled at

10,000 Hz. To obtain the N20m response to median nerve stimuli, the data from 25 ms before to 175 ms after the stimulus onset were averaged 200 times. In subsequent off-line analysis, the averaged data were digitally band-pass filtered from 0.03 to 2,000 Hz. The N20m response was identified visually as the first prominent peak at 20.2 ± 1.5 ms (mean ± standard deviation) after the onset[12], with the isofield map showing anterior current orientation. The location of N20m source was estimated at the peak latency, using a model of equivalent current dipole with the best fit sphere for a subject's head[27]. The source was superimposed on a three-dimensional MR image of the subject (Fig. 3d) using a MEG-MR image coordination integration system (MEG Laboratory; Ricoh), as well as used for simulation maps of both radial and tangential MEG measurement (Fig. 2).

TMR-MEG system.

Figure 1 shows a photograph and the schematic image of the developed TMR sensor with 74 MTJs, a facing pair of T-shaped MFCs and the measurement circuit diagram used for the MEG measurement. Device area of a MTJ was 50 × 50 μm^2. Length of the series array of 74 MTJs was 6.7 mm. MTJ multilayer films were deposited on thermally oxidized Si wafers using an ultrahigh-vacuum ($P_{base} < 1 \times 10^{-6}$ Pa) sputtering system. The stacking structure was Sub. Si, SiO_2/bottom electrode/$Co_{70.5}Fe_{4.5}Si_{15}B_{10}$ 140/Ru 0.4/$Co_{40}Fe_{40}B_{20}$ 3/MgO/$Co_{40}Fe_{40}B_{20}$ 3/Ru 0.9/$Co_{75}Fe_{25}$ 2/$Ir_{22}Mn_{78}$ 10/Ta 5/Pt 5/Ru 5 (in nm). The bottom CoFeSiB and CoFeB free layers show weak magnetic coupling, and the magnetization reversal process reflects that of the thick CoFeSiB layer with excellent soft magnetic properties[10,28]. For the preparation of very thin MgO barriers, the Mg layer of 0.7 nm was deposited on top of the bottom CoFeB layer and then oxidized by pure oxygen in the deposition chamber. To fully oxidize the Mg layer and obtain the intended thickness of the MgO barrier, the process of depositing Mg layers and in-situ natural oxidization was repeated several times sequentially[23]. The prepared MTJ multilayer films were microfabricated into MTJ arrays by photolithography and Ar ion milling. The TMR sensor has a structure in which 74 MTJs with device area of 50 × 50 μm^2 are connected in series to reduce the 1/f noise[29–31] and the length of the 74 MTJ array is 6.7 mm. After the microfabrication, the MTJ arrays were annealed using the double annealing process with a magnetic field of 0.3 T to realize linear output response against the external magnetic field[32]. The first and second annealing temperatures were 330˚C and 225˚C, respectively. The output of the TMR sensor predominantly changes with magnetic field applied in the short-side direction (sensing axis) of the MTJ array. On both sides of the MTJ arrays, a T-shaped MFC, which is effective for concentrating the external magnetic field[33,34], was prepared as shown in Fig. 1. The MFCs of 300-nm-thick $Fe_{73.5}Cu_{1.0}Nb_{3.0}Si_{15.5}B_{7.0}$ films were deposited, and 0.5-mm-thick $Ni_{80}Fe_{20}$ plates with T-shape were subsequently placed on the $Fe_{73.5}Cu_{1.0}Nb_{3.0}Si_{15.5}B_{7.0}$ films. The T-shaped MFCs have a size of 12.5 mm in the direction of the sensing axis (vertical line of "T") and 26.0 mm in the direction parallel to the MTJ array (horizontal line of "T").

A TMR sensor was used as one of the resistors in the bridge circuit, and its output voltage was amplified and filtered. The bridge was supplied with ±0.2 V, so the bias voltage of about 0.2 V was applied to the TMR sensor. The circuit to receive the signal from the bridge consisted of our homemade amplifiers and capacitor-resistor passive filters. The biomagnetic field signal measured by the TMR sensor was input to a two-stage amplification circuit with a total gain of 120 dB and passed through an analog bandpass filter from 0.8 Hz to 2 kHz. The signal output of the fabricated sensor system was 2.36 V/nT. The amplified and filtered signals were recorded on a PC at sampling rate of 2 kHz using an ADInstruments PowerLab 16/35 and LabChart8 software. The magnetic field signals were filtered in the software with a moving average (digital filter) from 20 Hz to 200 Hz. The pulse signal of the stimulation was also measured using the analog-to-digital converter at the same time, and the MEG was integrated 9,000 times by using the rising edge of the pulse as a trigger.

The sensitivity of our new TMR sensor was 940 fT/√Hz at 1 Hz, 200 fT/√Hz at 10 Hz, and 50 fT/√Hz at 1 kHz, which is about 100 times better compared to conventional magneto-resistive sensors[15], and none of the previous magneto-impedance sensors[16], fluxgate sensors[17], or diamond quantum sensors[18] have reached the high sensitivity level of our TMR sensors.

Simulation of TMR and SQUID-MEGs.

The TMR sensor used in this study has sensitivity in the horizontal direction of the scalp, which is different from the measurement direction of SQUID-MEG. Therefore, the tangential and radial magnetic flux densities generated by the N20m current were compared by simulations. The magnetic flux density on the scalp surface and SQUID measurement surface was calculated using the finite element method. The scalp model was an ellipsoid with radii of 10.3 cm in the front-back direction, 8.0 cm in the left-right direction, and 8.0 cm in the up-down direction, based on MR images and actual measurements, and the magnetic flux density was calculated when the measurement surface moved away from the scalp by 0.5 to 2.0 cm. The measurement surface of the SQUID-MEG was a sphere with a radius of 12.2 cm. The current of N20m in the brain was shaped as a thin cylinder with a length of 0.1 cm and a base area of 1 cm^2. The position and direction of the current were determined from the results of SQUID-MEG and MR imaging measurements. The magnitude of the current was adjusted so that the magnetic flux density in the radial direction matched the results of SQUID-MEG measurements. Here, the depth of the N20m current from the scalp was 2.4 cm at the shortest distance. The calculated magnetic flux density was plotted in two components: perpendicular to the N20m current on the scalp surface, and in the radial direction of the scalp. The plot perpendicular to the current on the scalp surface corresponds to the actual measurement direction of the TMR sensor, and the radial plot corresponds to the measurement direction of SQUID-MEG.

Measurement of median nerve SEFs by TMR-MEG system.

The subject underwent the same electrical stimulation in a magnetically shielded room as used in the previous SQUID-SEFs measurements. First, the subject wore a swimming cap to prevent any disruption

caused by the hair, fixed with elastic tape. Second, the TMR sensor was placed at the current dipole position determined by the SQUID SEFs. Next, the TMR sensor was repositioned at 1-mm and 1-degree intervals to find the maximum amplitude. Finally, the TMR sensor was placed at a position perpendicular to the active current direction to determine the maximum horizontal sensitivity to the scalp.

Declarations

Data Availability

The data that support the findings in this study are available from the corresponding author on reasonable request.

Author Contributions

A.K. and N.N. conceived the project, contributed data collection, data analysis and data interpretation, and wrote the paper. M.O. and K.F. contributed system design and fabrication, contributed data simulation, and wrote the paper. T.N. and T.A. contributed system design and fabrication. H.M. and Y.A. contributed conceptualization, system design and fabrication, and data interpretation.

Competing interests

N.N. served as paid consultant to Spin Sensing Factory Corp. K.F. is an employed researcher at Spin Sensing Factory Corp. T.A. is an employed researcher at KONICA MINOLTA, INC. H.M. serves without payment as president and director of Spin Sensing Factory. Y.A. serves without payment as a board member of Spin Sensing Factory and owns stocks of Spin Sensing Factory. No other authors declare individual competing interests.

Additional information

Correspondence and requests for materials should be addressed to N.N.

Reprints and permissions information is available at www.nature.com/reprints.

References

1. Hari, R. & Puce, A. *MEG-EEG Primer*. Oxford University Press, New York (2017).

2. Hämäläinen, M., Hari, R., Ilmoniemi, R. J., Knuutila, J. & Lounasmaa, O. V. Magnetoencephalography–theory, instrumentation, and applications to noninvasive studies of the working human brain. *Rev. Mod. Phys.* **65**, 413-497 (1993).

3. Geselowitz, D. B. On the magnetic field generated outside an inhomogeneous volume conductor by internal current source. *IEEE. Trans. Magn.* **MAG-6**, 346-347. https://ieeexplore.ieee.org/document/1066765 (1970).

4. Pfeiffer, C., et al. A 7-channel high-T_c SQUID-based on-scalp MEG system. *IEEE Trans. Biomed. Eng.* **67**, 1483-1489 (2020).

5. Riaz, B., Pfeiffer, C. & Schneiderman, J. F. Evaluation of realistic layouts for next generation on-scalp MEG: spatial information density maps. *Sci. Rep.* **7**, 6974 (2017).

6. Boto, E., et al. Moving magnetoencephalography towards real-world applications with a wearable system. *Nature* **555**, 657–661 (2018).

7. Knappe, S., Sander, T. & Trahms, L. Optically pumped magnetometers for MEG. In: Supek, S. & Aine, C. J. (eds). *Magnetoencephalography. Second Edition.* Springer Nature Switzerland AG, Cham, Switzerland, 1301-1312 (2019).

8. Miyazaki, T. & Tezuka, N. Giant magnetic tunneling effect in Fe/Al_2O_3/Fe junction. *J. Magn. Magn. Mater* **139**, L231-L234 (1995).

9. Moodera, J. S., Kinder, L. R., Wong, T. M. & Meservey, R. Large magnetoresistance at room temperature in ferromagnetic thin film tunnel junctions. *Phys. Rev. Lett.* **74,** 3273-3276 (1995).

10. Fujiwara, K., et al. Magnetocardiography and magnetoencephalography measurements at room temperature using tunnel magneto-resistance. *Appl. Phys. Express* **11**, 023001. https://doi.org/10.7567/APEX.11.023001 (2018).

11. Hari, R., et al. IFCN-endorsed practical guidelines for clinical magnetoencephalography (MEG). *Clin. Neurophysiol.* **129**, 1720-1747 (2018).

12. Kawamura, T., et al. Neuromagnetic evidence of pre- and post-central cortical sources of somatosensory evoked responses. *Electroencephalogr. Clin. Neurophysiol.* **100**, 44-50 (1996).

13. Nakasato, N., et al. Cortical mapping using an MRI-linked whole head MEG system and presurgical decision making. *Electroencephalogr. Clin. Neurophysiol. Suppl.* **47**, 333-341 (1996).

14. Ishida, M., et al. Awake state-specific suppression of primary somatosensory evoked response correlated with duration of temporal lobe epilepsy. *Sci. Rep.* **10**, 15895 (2020).

15. Cardoso, S., et al. Magnetic tunnel junction sensors with pTesla sensitivity. *Microsyst. Technol.* **20**, 793-802. https://doi.org/10.1007/s00542-013-2035-1 (2014).

16. Uchiyama, T. & Ma, J. Design and demonstration of novel magnetoencephalogram detectors. *IEEE Trans. Magn.*, **55**, 4400408. https://ieeexplore.ieee.org/document/4400408 (2019).

17. Lu, C. C. & Huang, J. A 3-axis miniature magnetic sensor based on a planar fluxgate magnetometer with an orthogonal fluxguide. *Sensors (Basel)* **15**, 14727-14744 (2015).

18. Herbschleb, E. D., Kato, H., Makino, T., Yamasaki, S. & Mizuochi, N. Ultra-high dynamic range quantum measurement retaining its sensitivity. *Nature Commun.* **12**, 306 (2021).

19. Nakasato, N., et al. Functional localization of bilateral auditory cortices using an MRI-linked whole head magnetoencephalography (MEG) system. *Electroencephalogr. Clin. Neurophysiol.* **94**, 183-190 (1995).

20. Yu, H. Y., et al. Neuromagnetic separation of secondarily bilateral synchronized spike foci: report of three cases. *J. Clin. Neurosci.* **11**, 644-648 (2004).

21. Scherg, M. & Buchner, H. Somatosensory evoked potentials and magnetic fields: separation of multiple source activities. *Physiol. Meas.* **14 Suppl 4A**, A35-A39. (1993).

22. Nakasato, N. Biomagnetometry is warming up from liquid helium to room temperature. *Clin. Neurophysiol*. **132**, 2666-2667 (2021).

23. Yuasa, S., Nagahama, T., Fukushima, A., Suzuki, Y. & Ando, K. Giant room-temperature magnetoresistance in single-crystal Fe/MgO/Fe magnetic tunnel junctions. *Nat. Mater.* **3**, 868-871 (2004).

24. Iwasaki, M., et al. Somatosensory evoked fields in comatose survivors after severe traumatic brain injury. *Clin. Neurophysiol.* **112,** 205-211 (2001).

25. Usubuchi, H. et al. Effects of contralateral noise on the 20-Hz auditory steady state response-magnetoencephalography study. *PLoS One* **9**, e99457 (2014).

26. Kawase, T. et al. Impact of audio-visual asynchrony on lip-reading effects—Neuromagnetic and psychophysical study. *PLoS One* **11**, 40 (2016).

27. Sarvas, J. Basic mathematical and electromagnetic concepts of the biomagnetic inverse problem. *Phys. Med. Biol.* **32**, 11–22 (1987).

28. Kato, D. et al. Fabrication of magnetic tunnel junctions with amorphous CoFeSiB ferromagnetic electrode for magnetic field sensor devices. *Appl. Phys. Express* **6**, 103004 (2013).

29. Tondra, M, et al. Picotesla field sensor design using spin-dependent tunneling devices. *Appl. Phys.* **83**, 6688 (1998).

30. Fujiwara, K. et al. Detection of sub-nano-tesla magnetic field by integrated magnetic tunnel junctions with bottom synthetic antiferro-coupled free layer. *Jpn. J. Appl. Phys*. **52**, 04CM07 (2013).

31. Deak, J. G., Zhou, Z, & Shen, W. Tunneling magnetoresistance sensor with pT level 1/f magnetic noise. *AIP Adv*. **7**, 056676 (2017).

32. Fujiwara, K., et al. Fabrication of magnetic tunnel junctions with a bottom synthetic antiferro-coupled free layers for high sensitive magnetic field sensor device. *J. Appl. Phys.* **111**, 07C710.

https://doi.org/10.1063/1.3677266 (2012).

33. He, G., et al. PicoTesla magnetic tunneling junction sensors integrated with double staged magnetic flux concentrators. *Appl. Phys. Lett.* **113**, 242401. https://doi.org/10.1063/1.5052355 (2018).

34. Zhang, X., et al. Influence of size parameters and magnetic field intensity upon the amplification characteristics of magnetic flux concentrators, *AIP Adv.* **8**, 125222. https://doi.org/10.1063/1.5066271 (2018).

Figures

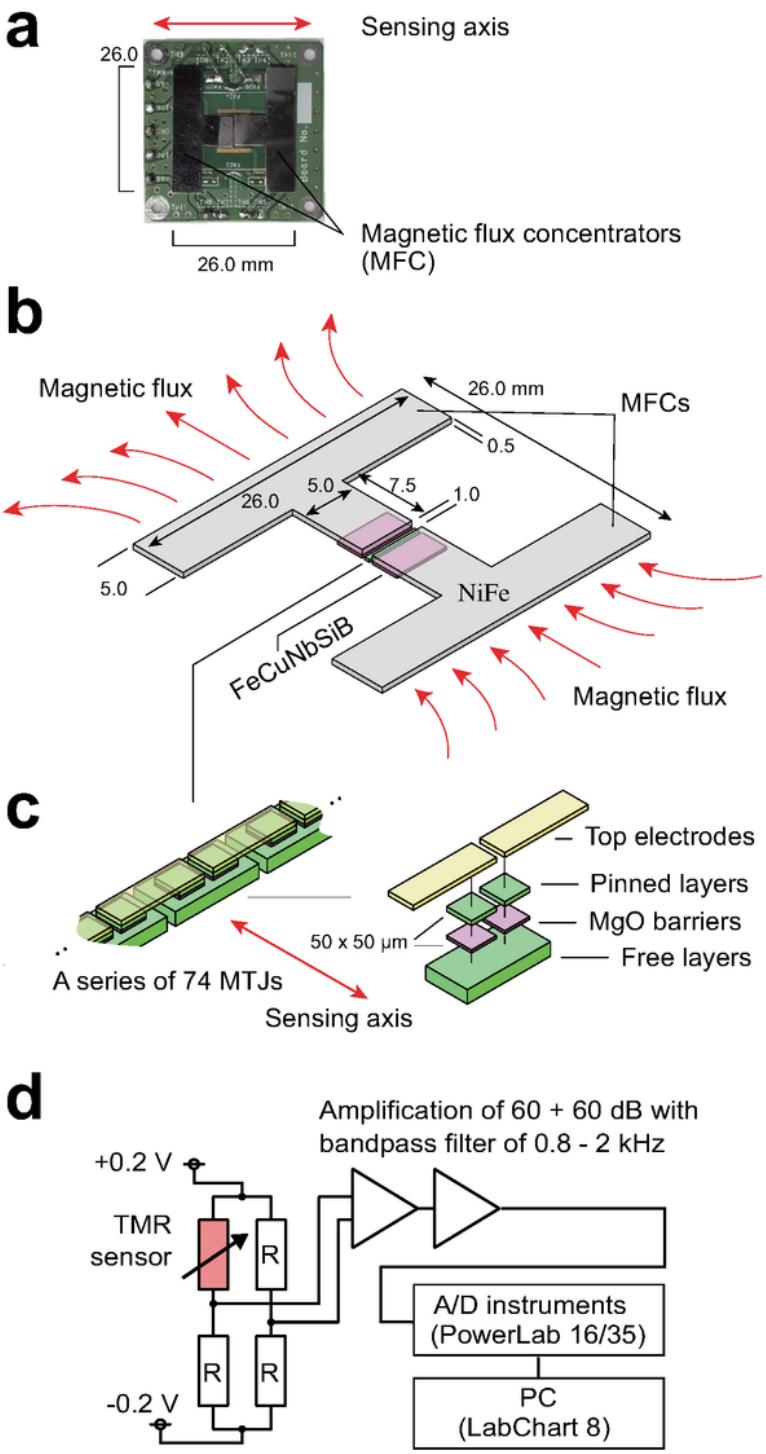

Figure 1

The TMR sensor system used for scalp-attached tangential MEG. a, Photograph of a TMR-MEG system consisting of two T-shaped MFCs (black) mounted on a circuit board. b, Schema of two MFCs fabricated by two film deposition of 300 nm-thick FeCuNbSiB in a size of 5.0 mm x 2.5 mm (purple) and a facing pair of T-shaped 0.5 mm-thick NiFe plates with 26.0-mm width (gray) parallel to the array of 74 MTJ (green). c, Partial and magnified schemas of the array of 74 MTJs. Resistance changes, across pinned

and free layers (green) separated by thin MgO barriers (purple), represent the scalp surface tangential MEG through MFCs. Top electrodes (yellow) connect the MTJs into a bridge circuit, amplifiers, and a signal analysis computer. d, Measurement circuit diagram used for the MEG measurement. A TMR sensor was used as one of the resistors in the bridge circuit, and its output voltage was amplified and filtered. The bridge was supplied with ±0.2 V, so the bias voltage of about 0.2 V was applied to the TMR sensor. The circuit to receive the signal from the bridge consisted of our homemade amplifiers and capacitor-resistor passive filters. The biomagnetic field signal measured by the TMR sensor was input to a two-stage amplification circuit with a total gain of 120 dB and passed through an analog bandpass filter from 0.8 Hz to 2 kHz. The amplified and filtered signals were recorded on a PC at sampling rate of 2 kHz using an ADInstruments PowerLab 16/35 and LabChart8 software. The magnetic field signals were filtered in the software with a moving average (digital filter) from 20 Hz to 200 Hz.

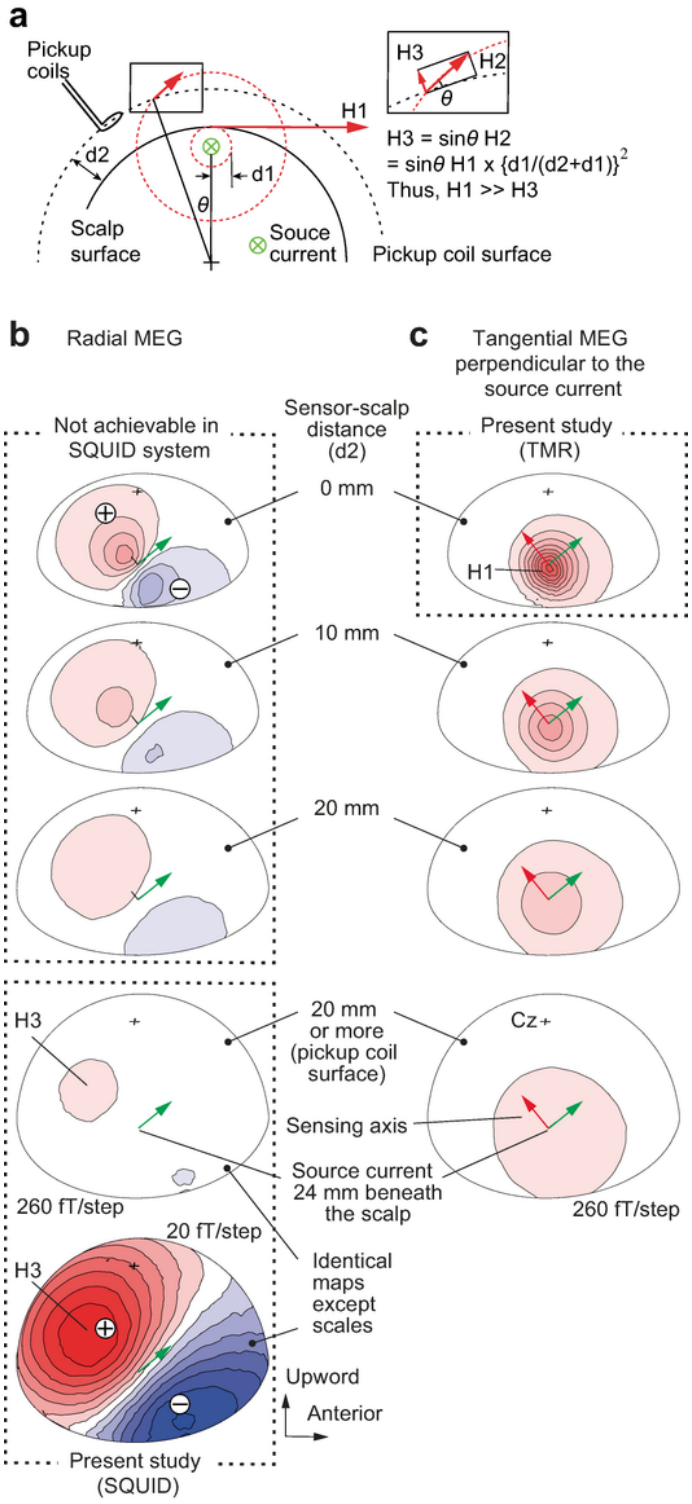

Figure 2

Advantages of scalp-attached tangential MEG. a, Schema to explain the difference in amplitude maxima between scalp-attached tangential MEG measured by TMR sensors (H1), unmeasured oblique MEG (H2), and scalp radial MEG measured at the pickup coil surface of SQUID (H3). Note the H1 amplitude is much larger than H3 under the Bio-Savart law showing the magnetic field generated by a current is negatively correlated to the square of source-sensor distance (d1 for H1 and d1+d2 for H2). b, Right parietal view of

simulated isofield maps of radial MEG at 4 different setback distances between the sensors and the scalp. A current source positioned 24 mm beneath the scalp simulating the N20m response after the left median nerve stimulation demonstrated in the present study. Note the clear dipole patterns of short inter-peak distances between magnetic influx and outflux, measured at 0, 10, and 20 mm above the scalp, are not achievable with superconducting MEG due to the wall thickness of the Dewar vessel containing liquid helium. c, Simulation of tangential MEG maps when measured perpendicularly to the source current. Note the largest and steepest peak on the scalp immediately above the source (H1) proved in the present study.

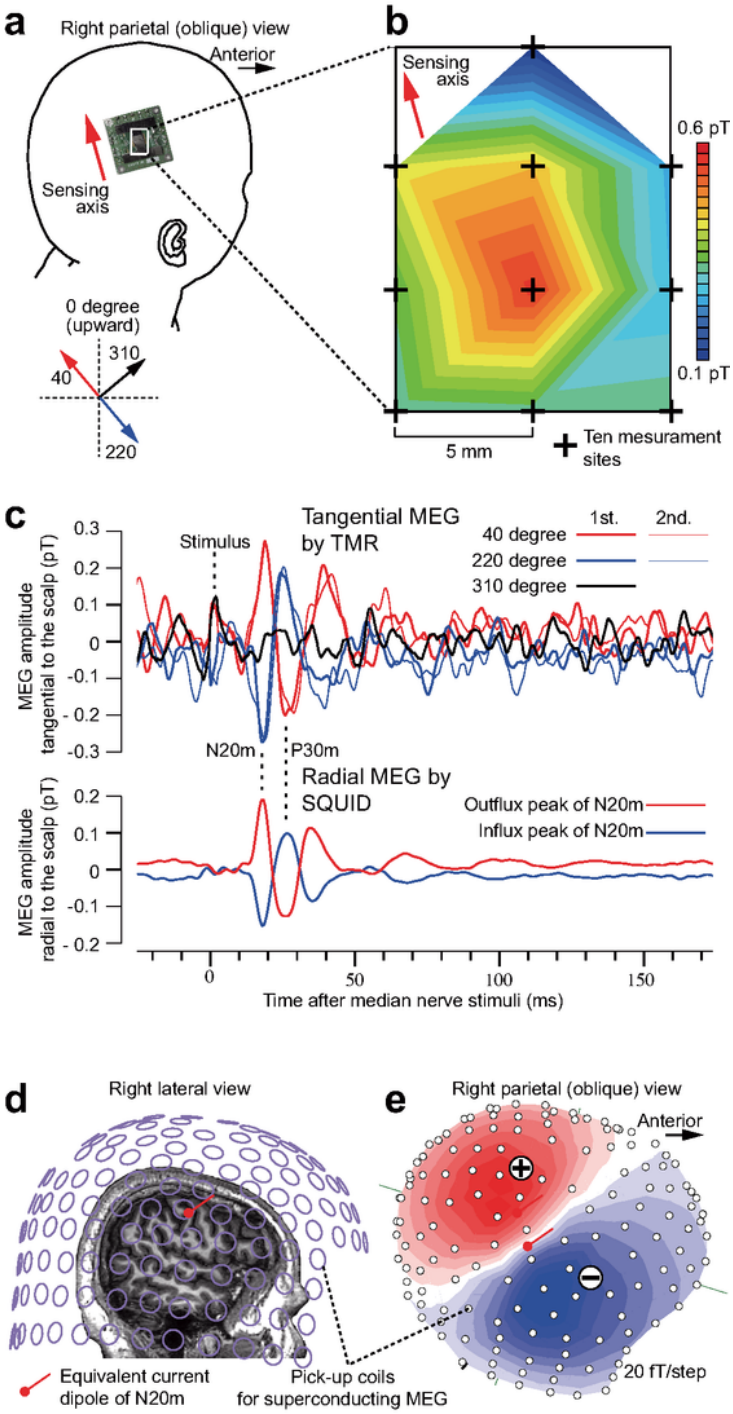

Figure 3

Comparison of tangential MEG using TMR sensors and radial MEG using SQUIDs to measure SEFs in a healthy subject. a, Photograph of a single channel TMR-MEG system placed on the scalp over the right parietal area. Scalp-attached MEG was performed at 2.63 mm from the scalp to the center of the magnetic sensing point. b, Isofield map of N20m, the first SEF component for the left median nerve stimulation, measured at 10 different sites with identical sensing axis of 40 degree counterclockwise

from superiorly. Note the spatially steep peak of the N20m. c, Representative SEF waveforms measured by scalp-attached tangential TMR-MEG along three different sensing axes (top) and by the helmet-shaped 200-channel superconducting MEG system (bottom). The 1st and 2nd lines represent two different averaging sessions (N = 9,000) to show waveform reproducibility in TMR-MEG for the first (N20m) and second (P30m) components of SEFs comparable to superconducting MEG. d, The helmet-shaped 200-channel radial SQUID-MEG and the equivalent current dipole of N20m superimposed on a sagittal magnetic resonance (MR) image of the subject. Note the setback distance between the pickup coils and the scalp due to the Dewar vessel containing liquid helium. A red circle and a bar respectively indicate position (on the central sulcus) and orientation (anterior and superior) of the N20m dipole. e, Isofield map of N20m measured by a helmet-shaped 200-channel radial SQUID-MEG. N20m dipole is projected to the coil surface.